Relationship between the Aerodynamic Roughness Length and the Roughness Density in Cases of Low Roughness Density*

F. MINVIELLE[a], B. MARTICORENA[a], D.A. GILLETTE[b,**], R.E. LAWSON[b], R. THOMPSON[b] and G. BERGAMETTI[a]

[a]*Laboratoire Interuniversitaire des Systèmes Atmosphériques, Créteil, France*
[b]*Air-Surface Processes Modeling Branch, Atmospheric Sciences Modeling Division, Air Resources Laboratory, National Oceanic and Atmospheric Administration, Research Triangle Park, NC, USA, on assignment to the U.S. Environmental Protection Agency, Research Triangle Park, NC, USA*

Abstract. This paper presents measurements of roughness length performed in a wind tunnel for low roughness density. The experiments were performed with both compact and porous obstacles (clusters), in order to simulate the behavior of sparsely vegetated surfaces. The experimental results have been used to investigate the relationship between the ratio z_0/h and the roughness density, and the influence of an obstacle's porosity on this relationship. The experiments performed for four configurations of compact obstacles provide measurements of roughness length z_0 for roughness densities λ between 10^{-3} and 10^{-2} which are in good agreement with the only data set available until now for this range of low roughness densities. The results obtained with artificial porous obstacles suggests that the aerodynamic behavior of such roughness elements can be represented by the relationship established for compact obstacles, provided a porosity index has been used to determine the efficient roughness density (the fraction of the silhouette area actually sheltered by solid elements) rather than counting the porous object as solid. However, the experiments have been performed with relatively low porosity indices (maximum = 25%) for which the porosity has a negligible influence. In this range of porosity index, representing the aerodynamic behavior of porous obstacles using the relationship established for compact obstacles, should not lead to a significant error. However, the influence of the porosity may be important for porosity indices larger than 30%.

1. Introduction

Wind erosion in arid and semi-arid regions is a major source of tropospheric aerosols [1]. During transport through the atmosphere, these soil-derived particles strongly affect the radiative budget by backscattering and absorbing incoming (visible) and outgoing (infra-red) radiation [2, 3]. Moreover, recent works [2, 4] suggest that dust emissions in semi-arid regions could increase due to human or climatic disturbances such as overgrazing or drought.

Aeolian erosion occurs only when a threshold value of the wind velocity is reached (alternately, when the threshold friction velocity u_{*t} is exceeded. Because this threshold depends on the surface features, it exhibits very different values over the various arid and semi-arid surfaces. As a result, dust emissions are sporadic and spatially heterogeneous, making difficult any precise assessment of their impacts. Thus, modeling is one of the most adequate approaches to quantifying the dust emissions over arid and semi-arid areas.

A dust emission model representing the influence of wind velocity and soil surface features has been developed for large-scale applications [5, 6]. It includes a physical parameterization of the threshold friction velocity (the key parameter of the erosion processes) based mainly on a drag partition scheme in which the wind energy is transferred to the erodible surface as a function of the surface roughness length. This parameterization was found to adequately reproduce the threshold friction velocities (at which wind erosion commenced) measured on a variety of natural surfaces–from smooth, erodible surfaces to rough surfaces well protected from erosion [7].

Precise estimations of dust emissions from semi-arid areas require parameterizations accounting for the influence of seasonal precipitation on erosion thresholds. Precipitation has two main effects:

(1) Soil moisture increases the erosion thresholds by reinforcing soil cohesion. One example of this is in the dust emission model of Fécan *et al.* [8].

(2) Precipitation allows the growth of seasonal vegetation, which increases the surface roughness and thus absorbs a part of the wind energy.

To model the influence of vegetation on wind erosion threshold velocities, it is necessary (a) to describe quantitatively any variations in the amount of vegetation and (b) to represent the additional roughness due to vegetation. The first point can be achieved by using a model describing the growth of seasonal vegetation. As an example, the model developed by Mougin *et al.* [9] simulates total biomass, height, and surface cover fraction of grassland vegetation as a function of environmental variables. This model has been applied and validated for Sahelian regions [10]. The second point requires the estimation of aerodynamic roughness length caused by the vegetation. To make this estimation, the necessary information concerning the amount of vegetation and its geometrical characteristics is derived from the vegetation model.

A relationship linking the aerodynamic roughness length to the geometrical characteristics and density of obstacles has been established for artificial compact elements based on wind tunnel observations [6]. This empirical relation reproduces the experimental data with a good confidence level. However, it is not obvious that it can be applied to describe the aerodynamic behavior of the vegetation, since this relation concerns solid obstacles while vegetation exhibits specific characteristics unrelated to solid obstacles such as porosity and flexibility.

The aim of this work is to examine the possibility of using similar relationships to estimate roughness length due to vegetation, and to evaluate the possible influ-

ence of one of the main structural characteristics of vegetation: porosity. This study will be based on wind tunnel measurements of aerodynamic roughness length for a range of low roughness densities (sparse vegetation), using both compact and porous artificial obstacles.

2. Statement of the Problem

A particle of soil can be entrained into the air by the wind friction stress, provided this force is stronger than the added effects of particle weight and interparticle cohesion force. The equilibrium between these three components defines the erosion threshold of a particle, in terms of either the wind friction stress τ or the corresponding wind friction velocity u_{*t}. The dependence of the threshold u_{*t} as a function of the particle diameter D_p has been largely documented, based on wind-tunnel experiments [11] for a smooth, erodible surface. However, natural arid surfaces are often covered with a variety of small-scale obstacles such as gravels, pebbles, stones, rocks, and elements of vegetation. These objects absorb part of the atmospheric momentum and oppose erosion. The resulting erosion threshold u_{*t} therefore increases with increasing surface roughness.

Various parameterizations of the increase in erosion threshold as a function of surface roughness have been developed. Based on a dimensional analysis of the fractions of wind stress absorbed by nonerodible roughness elements and intervening erodible soil, [12] and Raupach *et al.* [13] proposed a parameterization of the threshold friction velocity as a function of roughness density, λ, defined as the mean frontal area of the roughness elements. For a plan surface S with n rectangular obstacles of mean width b and mean height h, the roughness density is expressed as follows:

$$\lambda = \frac{nbh}{S}. \tag{1}$$

An alternative specification of the drag partition, uses aerodynamic roughness length z_0 [5]. The parameter z_0 is the length scale that characterizes the loss of wind momentum attributable to the roughness elements and is an integrative parameter that represents the effect of the roughness elements.

In neutral conditions, the roughness length can be derived from the vertical logarithmic profile of the wind velocity:

$$U(z) = \frac{u_*}{k} \ln\left(\frac{z}{z_0}\right), \tag{2}$$

where $u_*{}^*$ is the friction velocity, k is the Von Karman constant (k = 0.4), z is the height, z_0 is the roughness length.

Numerous authors have proposed relationships between the aerodynamic roughness length and the roughness density. For roughness density greater than 0.11, a

simple relationship $z_0/h = 1/C$ (with C ranging from 7 to 30) is generally shown by data [14, 15]. For roughness densities less than 0.11, Lettau [14] proposed a linear relation between Z_0, λ and h, formally justified by Wooding *et al.* [16]:

$$\frac{Z_0}{h} = \frac{\lambda}{2}. \tag{3}$$

Based on measurements for roughness elements of various forms and dimensions, Marticorena *et al.* [6] derived the following empirical relationships between the ratios Z_0/h and λ.
For $\lambda < 0.11$:

$$\frac{Z_0}{h} = 10^{(1.33 \log \lambda - 0.03)}. \tag{4}$$

For $\lambda > 0.11$, z_0/h is considered constant and according to experimental values follows the relation

$$\frac{Z_0}{h} = \frac{\lambda}{2}. \tag{5}$$

Figure 1 shows the ratio Z_0/h as a function of λ for those measurements available in the literature.

As can be seen in Figure 1, the only measurements of roughness length available in the literature for vegetated surfaces (that is, of Hagen and Lyles, Musick and Gillette, Garratt, Raupach, Jarvis *et al.*, Wolfe and Nickling, and Wyatt and Nickling) correspond to roughness densities around or larger than 0.1. The only data set documenting a wide range of roughness density less than 0.1 was obtained by Marshall [17] for compact obstacles of various shapes and dimensions. The measurements of erosion thresholds over vegetated surfaces suggest that the results of Marshall [17], when applied to vegetation, tend to overestimate its protection effect [18–20]. This is a critical point for estimating wind erosion in semi-arid areas, since sparsely vegetated surfaces are the most easily erodible. For compact obstacles, Marshall's results [17] also show that the shape, the size, and the arrangement of obstacles have a negligible influence in comparison with the variations of roughness density. Musick *et al.* [21] confirmed that the simulation scale (ratio of simulated size to natural size) and the ratio of size (h/b) of obstacles play minor roles in increasing the erosion threshold. Finally, a possible explanation for the discrepancies between compact obstacles and vegetation could be the porosity, a structural factor characterizing the vegetation [21]. This factor is particularly important for the type of vegetation encountered in semi-arid zones, where the leaf cover can be very low or even negligible.

For a vegetation cluster, the silhouette area (which corresponds to the geometric frontal surface) is composed of both solid elements (branches and leaves) and the spaces between the elements. Consequently, for a given silhouette area, a vegetation cluster is different in terms of wind momentum loss than a solid obstacle, since
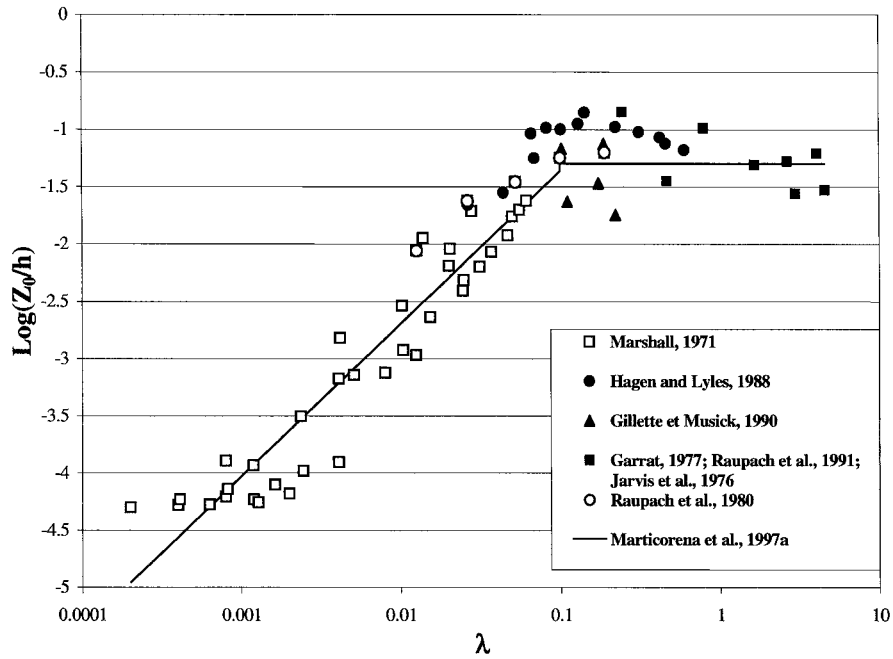
Figure 1. Ratio z_0/h as a function of the roughness density λ for compact obstacles (white symbols) and for vegetated surfaces (black symbols). Data from Raupach *et al.* [29] (cylinders of 6 mm and variable space between); Marshall [17] (cylinders and hemispheric obstacles of variable size and space between); Hagen and Lyles [27] (vegetation of semi-arid type: yucca and sagebrush); Musick and Gillette [20] (canopy vegetal); Garratt [26], Raupach [12], Jarvis *et al.* [28] (canopy vegetal and model of canopy vegetal in wind tunnel); Wolfe and Nickling [31] (Sonoran Desert); Wyatt and Nickling [32] (semi-arid vegetation: creosote from Nevada, Sagebushes, Prosopis); Marticorena *et al.* [6] (Equations (3) and (4)).

there is a different amount of actual obstacle surface interacting with the wind flow than the frontal surface represented by the silhouette area. This suggests that the roughness density computed from the geometric silhouette area for a very porous plant may overestimate the roughness effect of vegetation. Moreover, the experimental results from Nickling and Gillies suggest that drag coefficients for porous vegetation elements are quite complex because of pore and plant morphology, that can change as a functions of wind speed and Reynolds Number.

A possible way to correct this is to account for the porosity index P, which allows the calculation of an 'effective roughness density' λ_{eff} from the geometric roughness density $\lambda_{\text{geom.}}$ (Figure 2):

$$P = \frac{S_{geom.} - \sum s_i}{S_{geom.}}, \tag{6}$$

**Compact
obstacle**   **Artificial
porous obstacle**   **Effective frontal
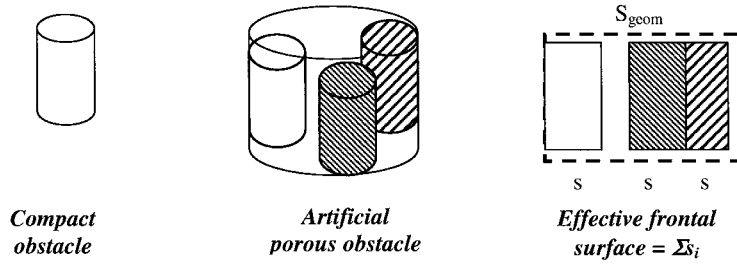surface = Σs_i**

Figure 2. Illustration of the definition of the effective frontal area for artificial porous obstacles.

where S_{geom} is the geometric silhouette area perpendicular to the ground of the vegetation cluster, and s_i is the frontal surface of the individual elements of the cluster;

$$\lambda_{geom} = \frac{n_c b_c h_c}{S_{geom}},$$

$$(7)$$

where b_c, h_c, and n_c are respectively the width and the height and the number of elements for the cluster silhouette area.

$$\lambda_{eff} = (1 - P).\lambda_{geom.}$$

$$(8)$$

Based on these definitions, P can only reach a maximum value of 1, when the geometric silhouette area is totally obstructed by individual compact elements. By making this definition, it is not allowed to exceed one, even if the sum of the frontal surface of the individual compact elements is higher than the geometric surface.

We have performed wind-tunnel experiments to investigate physical relationships between the geometric characteristics of vegetation and its aerodynamic roughness length. We will focus on roughness density corresponding to sparse vegetation, i.e roughness densities less than 0.1, and on the possible influence of the resulting porosity.

3. Experimental Strategy

3.1. WIND TUNNEL AND INSTRUMENTS

3.1.1. *Description of the Wind Tunnel*

The experiments were performed in the meteorological wind tunnel at the U.S. Environmental Protection Agency's Fluid Modeling Facility (Figure 3) [30].

The wind tunnel is of the open return type, with the test section 3.7 m wide, 2.1 m high, and 18.5 m long. The flow is produced by a 1.8 m-diameter axial flow fan driven by a 75 kW, 100 hp AC motor. The air enters the tunnel test section through a honeycomb flow straightener, four screens, and a contraction of length
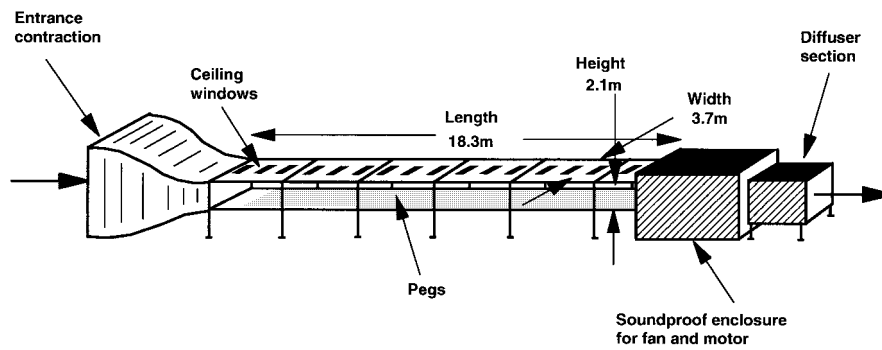
Figure 3. Schematic diagram of the EPA Meteorological Wind Tunnel.

of 3.3 m with a contraction ratio of 2.8:1. The air speed through the test section can be set from 0.5 to 10 m/s. The ceiling of the test section is adjustable in height to compensate for blockage effects due to large models or to compensate for the growth of a thick floor boundary layer. The height adjustment allows a nonaccelerating free stream flow. Downstream of the test section, the air passes through an acoustic silencer, a fan, a diffuser section, and a final acoustic silencer before being exhausted back into the laboratory. The boundary layer developed in the wind tunnel simulates a neutral atmospheric boundary layer.

The flow entering the test section was of uniform speed and low (less than 1%) turbulence intensity. The boundary layers studied here were grown naturally over the various patterns of pegs protruding from the floor (i.e., no boundary layer trip was used). The developed or equilibrium boundary layer (not changing with downwind distance) typically had a thickness (distance from surface to height at which the velocity was 99% of the uniform velocity above) about 500 mm and could be described by a logarithmic profile. Such boundary layers developed quickly, within a few meters of the test-section entrance. All velocity measurements were made at a nominal distance of 15 m downwind of the test-section entrance. The free stream wind speed, above the boundary layer, was set to 6.3 m s^{-1} for all experiments.

3.1.2. *Instrumentation*

A TSI Inc. IFA 100 hot-wire anemometer (the HWA) with single hot-wire probes (Figure 4) was used to measure wind velocity. This instrument is useful and convenient when the turbulence intensities are low. The probes are calibrated by placing the hot-wire probe close (130 mm) to a Pitot-static tube used as reference instrument, for flow velocity in the tunnel ranging from 0.75 to 7 m/s. The reference flow velocities are computed from the differences of pressures measured by a differential pressure sensor (MKS Baratron), connected to the Pitot-static tube. Output voltages from the hot-wire anemometer are recorded by a computer. The

Figure 4. Photograph of the hot wire probe.

calibration voltages are used to calculate a set of best-fit parameters to the King's law equation [25]:

$$E^2 = A + BU^\alpha, \tag{9}$$

where E is the anemometer output voltage, U is the mean wind velocity indicated by the Pitot-static tube, A, B, and α are constants determined using an in-house program, HCALX. Program HCALX uses a least-squares fit to obtain A and β for a specified range of α. Then the overall best fit is selected to give A, β and α.

The automated instrument carriage system positions the probe in the test section and may be controlled either by hand or by a microcomputer linked to the data acquisition computer. Software drives the three-dimensional movement of the probe and records its position in the section test with an accuracy of ± 1 mm. The analog signal of the hot wire anemometer was supplied to an analog-to-digital converter card (Data Translation model DT2801A, 12-bit) in the data acquisition minicomputer. The signal was digitized, linearized according to equation 9 above and processed to compute mean and root-mean-square values of velocity. At each velocity sampling location, an averaging time of 60 sec and a sampling rate of 1000 Hz were used and found to give repeatable values.

3.2. DESIGN OF THE EXPERIMENTS

3.2.1. *Dimensions of Obstacles and Range of Roughness Density*

The dimensions of the obstacles and the range of roughness density used for the experiments were chosen by considering the size of the wind tunnel and similarity requirements for scale-modeling of aerodynamic flows. The optimal height of obstacles was estimated to be on the order of 20 mm.

Because this study involves the measurement of neutral flow (and no particle motions), maintaining a sufficiently large Reynolds number is the only requirement for correct simulation of the turbulent full-scale flow. A compromise between the obstacle height (Reynolds number) and the length of the upwind fetch (required to naturally develop the boundary layer) was made with the selection of 25.5 mm high cylindrical obstacles. The wind tunnel was operated at free-stream air speed of 6 m/s, near its maximum, to produce the largest Reynolds number possible. Marshall [22] also used cylindrical pegs as roughness elements and found Reynolds number independence of his observations for Reynolds numbers of $1.5–3.0 \times 10^4$ based on the peg height and wind speed at z = 2H. The corresponding Reynolds number for this study was somewhat lower 8.5×10^3. However, Marshall points out that the flow around cylinders is relatively constant for $1.0 \times 10^3 < \text{Re} < 2 \times 10^5$ where the Reynolds number is based on the cylinder diameter [23, 24]. A Reynolds number computed from the diameter of our pegs and the flow speed at the height of the midpoint of the pegs is 2.5×10^3. The wind tunnel flow should simulate full-scale conditions.

We used commercially available pegs (longitudinally fluted woodworking dowels), 38 mm high and 9.5 mm diameter. The pegs were plugged in drilled plywood sheets of 12.5 mm thickness, so that the height of the pegs exposed to the flow was 25.5 mm. For this height, a maximum roughness density of about 0.03 was obtained by distributing 8064 obstacles over the total surface of the wind tunnel (63 m^2). Lesser densities were obtained by inserting fewer pegs.

The dimension of the wind tunnel required that a certain minimal number of elements be distributed over its total surface. From the experiments previously performed in this wind tunnel, it had been learned that a minimum number of one peg per 930 cm^2 is required to noticeably affect the surface roughness and influence the wind flow.

3.2.2. *Operational Set-Up*

The operational set-up was designed to facilitate change from one experiment (pattern of pegs) to another. It consisted of 21 sheets of plywood (1.2192 by 2.4384 m) placed along the test-section floor 3 abreast to obtain a total surface area of 62.43 m^2. A repeating pattern of holes within a square (304.8 mm by 304.8 mm) was chosen so that a 4 by 8 array of this pattern just filled each sheet of plywood and the pattern matched at the edges of neighboring sheets of plywood. This pattern was chosen to obtain a symmetric distribution of roughness elements across the total surface of the wind-tunnel floor. The hole pattern within each square is shown in Figure 5. Holes numbered 1 through 4 are located within the 304.8 mm square such that the repeating pattern of holes comprises a regular array with a uniform spacing of 152.4 mm over the entire test-section floor. Within each square, a rosette (please see Figure 7) made up of 8 holes drilled on a circle of 30-mm radius was centered on hole 1. Each rosette was rotated so that the most upwind hole was at an angle of 15° from the wind direction; this was to avoid pairs of pegs within
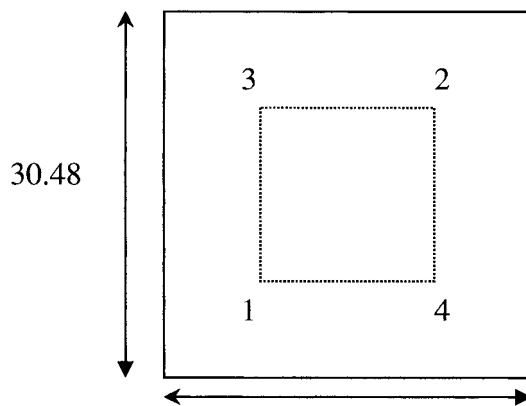
Figure 5. Square distribution used as design for the studied configurations. The distances between the four positions are 15.24 cm.

the rosette from being aligned with the wind direction. Each peg in the rosette contributed, by its frontal silhouette area to the absorption of wind energy.

For the first set of experiments concerning compact obstacles, three different roughness densities were obtained by placing a single peg at position 1, then one peg each at positions 1 and 2, then one peg each at positions 1, 2, 3, and 4 for each square foot. These cases, denoted C1, C2, and C3 are listed in Table I.

For the second set of experiments, only position 1 was used. Following Musick *et al.* [21], we designed an artificial porous obstacle: a cluster composed of short segments. The cluster consisted of pegs laid out in the rosette pattern: up to eight pegs were placed in the 30 mm radius circle with one peg at the center. Three different porosities were used for the clusters: (1) One peg at the center and two pegs on the rosette (three pegs in total); (2) two pegs added to (1) on the circle (five pegs in total); and (3) completion of the circle by four pegs added to (2) (nine pegs in total). Cases for these positions are listed as P3, P5, and P9 in Table I. The pegs in the rosettes were placed in the same positions for each square.

A last configuration was studied (CP12) in which all the available positions (8064 pegs) were occupied. This configuration provided the maximum value of λ for our experiments. This configuration was not spatially homogeneous.

3.3. EXPERIMENTAL PROCEDURE

Determination of aerodynamic roughness length is based on measurements of the flow velocity at various heights above the obstacles. Measurements of turbulence intensity are used to identify the positions of steady turbulence. This measurement determined the time needed to form averages for our measurements.

Table I. Configurations for all experiments.

Configuration number	Pegs per square	Total number of pegs
C1	1	672
C2	2	1344
C3	4	2688
P3	3	2016
P5	5	3360
P9	9	6048
CP12	12	8064

3.3.1. *Lateral Transect of Turbulence Intensity*

Lateral tranverses at z = 20 mm (slightly less than the height of the roughness elements) give the velocity and the turbulence intensity (u′/U) across the roughness pattern of pegs. The resulting profiles were used to identify areas where small traverses in the y direction did not result in much change of turbulence intensity where the measurements of vertical profiles were made. These lateral profiles were obtained at 48 mm behind the obstacles placed in the mid-point of the wind tunnel at a longitudinal distance of x = 15148 mm, extending over a width of about ± 300 mm from the lateral (width) midpoint. This distance covered the interval of three obstacles for the configuration of minimal density, and the interval of five obstacles for the maximal density. Figure 6 illustrates a lateral profile obtained for the case of porous obstacles, P9, from which we selected the relevant positions for the vertical profile measurements.

3.3.2. *Vertical Profiles of the Flow Velocity*

Vertical profiles were realized at four different longitudinal (x) positions, four or six lateral (y) positions, and 19 vertical (z) positions, between 5 mm and 800 mm from the floor of the wind tunnel. We kept, where possible, the same relative positions for the different configurations (measurement positions are given in figure 7). The positions x = 11000 mm (Pv1), and x = 13000 mm (Pv2) provided observations of the development of the boundary layer. These measurements confirmed that for the positions where the majority of measurements (x = 15000 mm (Pv3) and x = 15148 mm (Pv4)) were performed, the boundary layer was well established. The lateral positions (y) for the vertical profiles at x = 15000 mm and x = 15148 mm were chosen among the stable turbulent positions according to the lateral transect measurements. The positions y = 90 mm (Pv5), −225 mm (Pv6), and 150 mm (Pv7) were located between two obstacles (groups of 1 to 9 pegs). The positions
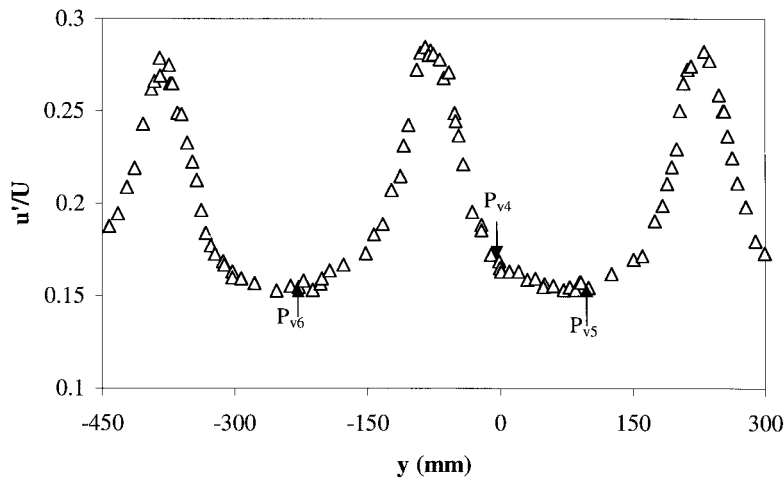
Figure 6. Lateral transect of turbulence intensity measured at z = 20 mm and x = 15148 mm, for the configuration P9 (porous obstacles). Black triangles correspond to the positions of steady turbulence selected for the vertical profiles measurements.

y = 0 mm (Pv4) and y = −300 mm (Pv8) are placed respectively at 50 mm and 100 mm from an obstacle.

The Fluid Modeling Facility program 'logfit' allows determination of the roughness length Z_o, and the friction velocity u_*, by an adjustment of the measurements on the logarithmic vertical profile (Equation (2)). The criteria of the best fit are defined by the least-square method. Each profile is fitted using data collected above the internal boundary layer, which develops between the obstacles, and below the free layer. This method leads to the selection of measurements heights between 3 cm and 10 cm. Figure 8 illustrates a measured wind profile and the best fit to the measurements.

4. Results and Discussion

4.1. INITIAL TESTS IN THE EMPTY WIND TUNNEL

To evaluate the roughness induced by the plywood sheets, the aerodynamic roughness length was determined for the surface of the empty wind tunnel and for the drilled plywood sheets. The Z_0 values for these two cases are respectively 0.0028 ± 0.0011 cm and 0.0031 ± 0.0004 cm. The surface covered with the drilled plywood sheets appears as slightly rougher than the empty tunnel; however, with regards to the experimental uncertainties the two values are very similar.

This value, Z_0, is larger by a factor of ten compared to the value measured by Marshall [17], which can be explained by a difference in the material used to cover the surface. This indicates that our experimental setup is not valid for situations for which the roughness length is lower than 0.003 cm.
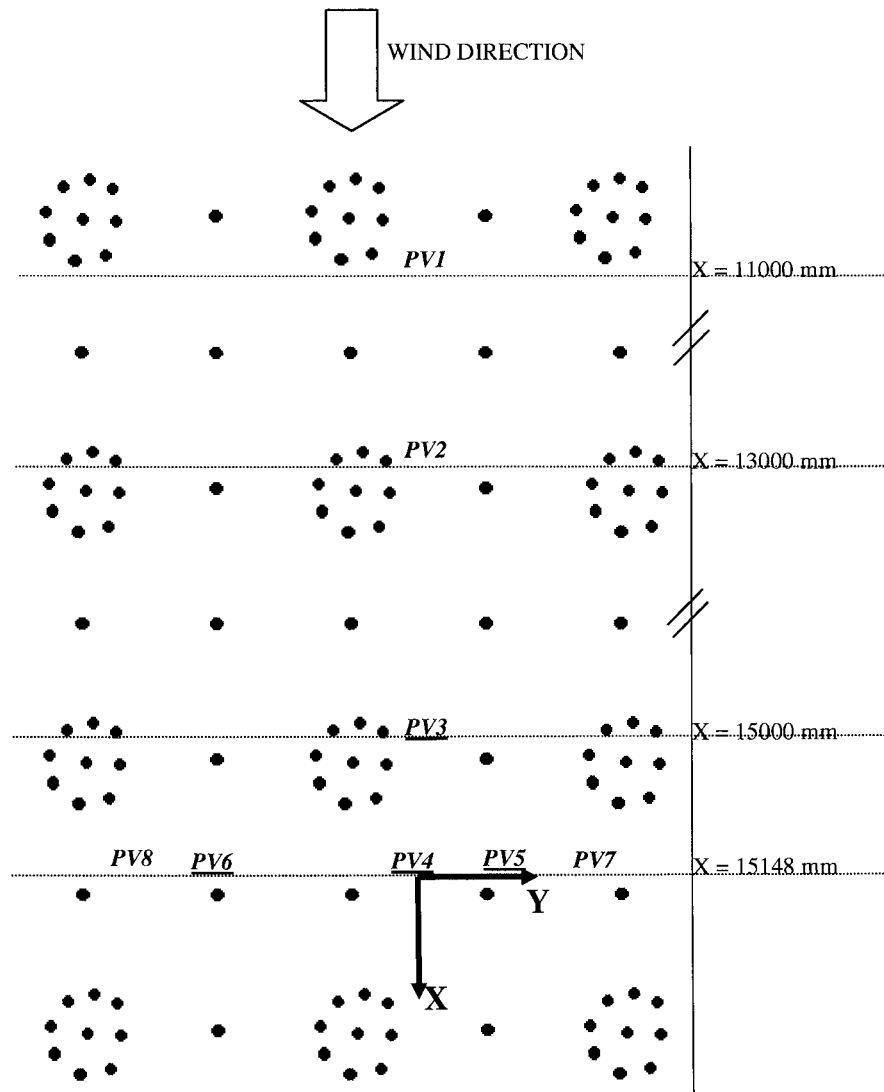
Figure 7. Lateral and longitudinal positions of measurements in the wind tunnel. The underlined symbols represent the positions where vertical profiles of velocity flow have been performed.

4.2. RESULTS OF EXPERIMENTS

4.2.1. *Solid Obstacles*

The results obtained for the first set of experiments are presented in Table II. The roughness densities have been computed from Equation (7) and have been displayed versus the total number of pegs for each configuration (Table I). The roughness lengths Z_0 have been determined at four positions of steady turbulence.
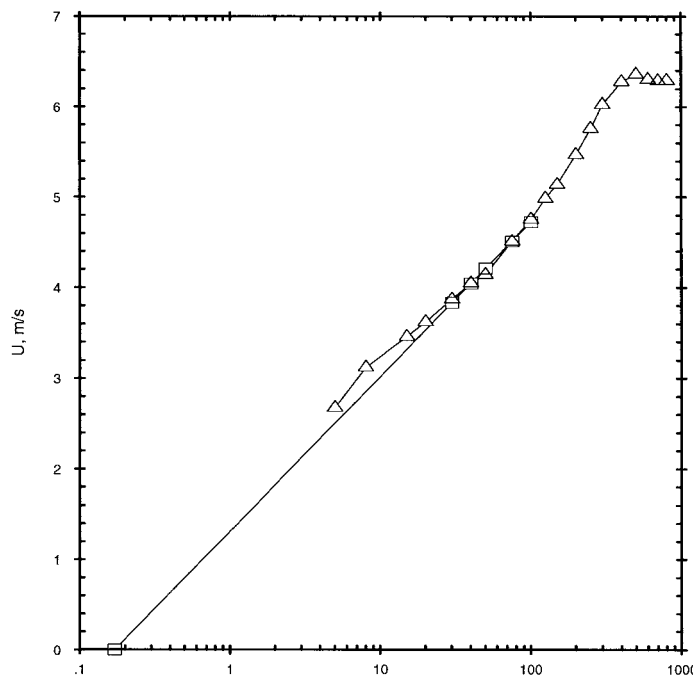
Figure 8. Vertical profile of wind velocity, measured for the configuration P4 (compact obstacles) for x = 15148 mm and y = 90 mm. Triangles correspond to wind velocity measurements, squares represent the data used for the fit of the logarithmic profile (straight line), and the square on the abscissa corresponds to the computed roughness length.

However, the sets of wind speed versus height for which the data were visually not log-linear were rejected from our data sets used to compute the mean roughness length.

The roughness densities computed for compact obstacles range over an order of magnitude but remain very low (from 0.00261 to 0.0267). The measured roughness lengths also vary on an order of magnitude (0.0035 to 0.04 cm). It must be noted that the number of data points used to determine the mean roughness length decreases when the roughness density is low. This is because the structure of the wind velocity profiles is not so well defined for low roughness densities.

The ratio Z_0/h, determined from the estimated roughness length, is plotted as a function of λ, for the four configurations C1, C2, C4, and CP12 (Figure 9). For comparison, the experimental data from Marshall [17] and the curves corresponding to Equations (3) and (4) were also reported.

The experimental data are in agreement with data from Marshall [17] and with the fitted Equations (4) and (5). The deviations of our points for this reference curve are of the same magnitude as for Marshall's [17] data.

Table II. Roughness densities $\lambda_{geom.}$, mean Z_0, number of data and standard deviation σ for the four configurations studied. The compact obstacles are individual dowel rods of 2.55 cm high and 0.953 cm wide.

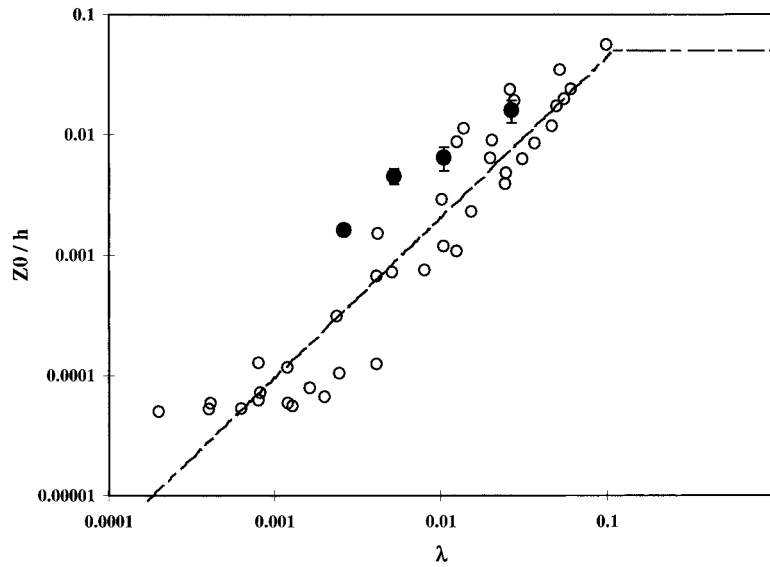| Number of configuration	$\lambda_{geom.}$	Mean Z_0 (cm)	Number of data	σ
C1	0.0026	4.109e-03	2	1.38e -04
C2	0.0052	1.163e-02	3	1.725e-03
C4	0.011	1.649e-02	4	3.608e-03
CP12	0.027	4.066e-02	8	8.516e-03

Figure 9. Ratio of roughness length and height of obstacles Z_0/h, as a function of the roughness density λ, determined for compact obstacles. Black circles represent the mean Z_0/h and the associated standard deviation; dashed lines correspond to Equations (4) and (5); white circles represent the measurements from Marshall [17].

4.3. POROUS OBSTACLES

The results obtained from the second set of experiments are presented in Table III. The porosity index, geometric roughness density and effective roughness density have been determined according to Equations (6), (7) and (8), respectively. They range from 0.0104 to 0.0189 for geometric roughness density ($\lambda_{geom.}$) and from 0.00823 to 0.0189 for effective roughness density ($\lambda_{eff.}$). Two of the artificial clusters have a porosity index on the order of 0.2. The last configuration is composed of a cluster with a porosity index of 0, which means that the projected silhouette area is totally covered by the separated individual elements composing the cluster.

Table III. Roughness densities $\lambda_{geom.}$ and $\lambda_{eff.}$, mean Z_0, number of data and standard deviation σ for the three configurations studied. The porous obstacles are clusters of individual dowel rods over widths of 3.8 cm, 6.6 cm, and 6.9 cm.

Number of configuration	Porosity	$\lambda_{geom.}$	$\lambda_{eff.}$	Mean Z_0 (cm)	Number of data	σ
P3	0.21	0.010	0.0082	5.98e -03	2	2.76e -03
P5	0.24	0.018	0.014	6.702e-03	3	1.742e-03
P9	0	0.019	0.019	8.385e-03	6	1.144e-03

The geometric roughness density and the geometric roughness density for the three configurations increase from configuration P3 to P9. The averaged ratios Z_0/h determined for the three configurations P3, P5, and P9 have been plotted as a function of the geometric roughness density $\lambda_{geom.}$ and of the effective roughness density $\lambda_{eff.}$ (Figure 10).

Compared to the compact obstacles, for equivalent geometric roughness densities the ratios z_0/h tend to be lower in the case of porous obstacles. When these ratios are plotted as a function of $\lambda_{eff.}$, we do not claim improved agreement with the values obtained for compact obstacles. This is owing to the small number of points with standard deviations large enough for the populations to overlap. The difference is not very large since the porosity indexes are relatively low (0.25 at maximum).

It is to be noticed that the Z_0/h values from the porous elements, is about a factor of 3 lower than the Z_0/h values for the compact elements for the same λ. The largest difference between the two groups is that the compact elements are uniformly spaced, while the porous elements are clustered in groups of 3, 5, or 9 elements.

For the studied cases, the maximum porosity is of the order of 25%, so the correction brought by a representation in effective roughness density is limited and could be neglected without adding a lot of uncertainty. This correction could be important for obstacles with porosity larger than 50%, where a difference of a factor 2 in the predicted Z_0/h can be expected from the extrapolation of our results to this range of porosity. This result could explain the overestimation of the protection effect of vegetation against aeolian erosion, which was based on measurements performed with compact obstacles [21].

5. Conclusion

This paper presents measurements of roughness length performed in a wind tunnel for situations of low roughness density, where aeolian erosion should be frequent. The experiments have been performed with both compact and porous obstacles
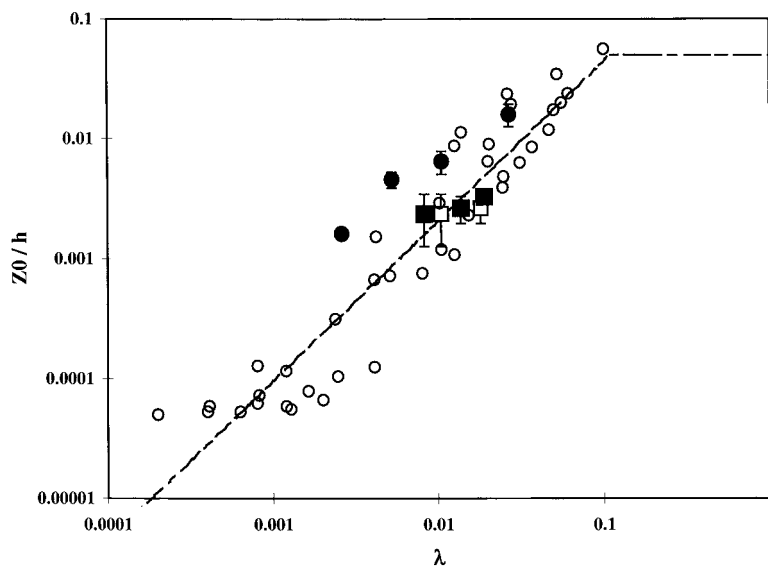
Figure 10. Ratio of roughness length and height of obstacles Z_0/h as a function of the geometric roughness density λ_{geom} (white squares) and as a function of the effective roughness density $\lambda_{eff.}$ (black squares) for porous obstacles. Symbols: Squares correspond to means ratio Z_0/h with the associated standard deviations; black circles correspond to the results obtained for compact obstacles; dashed lines correspond to Equations (4) and (5); white circles represent the measurements from Marshall [17].

(clusters), in order to simulate the behavior of sparsely vegetated surfaces. The experimental results have been used to investigate the relationship between the ratio Z_0/h and the roughness density, and the specific influence of an obstacle's porosity on this relationship.

The experiments performed for four configurations of compact obstacles provide measurements of roughness length Z_0 for roughness densities λ between 10^{-3} and 10^{-2}. The data are in good agreement with the only other data set available until now for this range of low roughness densities: that of Marshall [17]. This result confirms that the relation previously established between Z_0/h and λ [6] represents correctly the behavior of compact obstacles for low roughness densities.

If elements are clustered (into porous groups), the Z_0/h values fall by about the scatter of the Marshall values about his mean value. Consequently, clustering in groups of 3 to 9 reduces the Z_0/h value by about the same amount as a reduction of λ by a factor of 2 to 3.

These results suggest that this study should be extended by additional wind-tunnel measurements with porous obstacles having a larger porosity index. Moreover, the results from this wind-tunnel experiment should be compared to measurements from field experiments performed for surfaces with low roughness density and especially for sparsely vegetated surfaces.

Acknowledgement

References

1. Andreae, M.O.: 1994, Climate effect of changing atmospheric aerosol levels, In: A. Henderson-Sellers (ed.), *World Survey of Climatology*, Vol. XX, *Future Climate of the World*.
2. Andreae, M.O.: 1996, Raising dust in the greenhouse, *Nature* **380**, 389–390.
3. Li, X., Maring, H., Savoie, D., Voss, K. and Prospero, J.M.: 1996, Dominance of mineral dust in aerosol light scattering in the North-Atlantic trade winds, *Nature* **380**, 416–419.
4. Tegen, I., Lacis, A.A. and Fung, I.: 1996, The influence on climate forcing of mineral aerosols from disturbed soil, *Nature* **380**, 419–422.
5. Marticorena, B. and Bergametti, G.: 1995, Modeling the atmospheric dust cycle: 1. Design of a soil-derived dust emission scheme, *J. Geophys. Res.* **100**, 16415–16430.
6. Marticorena, B., Bergametti, G., Aumont, B., Callot, Y., N'Doumé, C. and Legrand, M.: 1997, Modeling the atmospheric dust cycle: 2-Simulation of Saharan sources, *J. Geophys. Res.* **102**, 4387–4404.
7. Marticorena, B., Bergametti, G., Gillette, D.A. and Belnap, J.: 1997b, Factors controlling threshold friction velocities in semi-arid areas of the United States, *J. Geophys. Res.* **102**, 23277–23288.
8. Fécan, F., Marticorena, B. and Bergametti, G.: 1999, Soil-derived dust emissions from semi-arid lands: 1. parameterization of the soils moisture effect on the threshold wind friction velocities, *Ann. Geophysicae* **17**, 149–157.
9. Mougin, E., Lo Seen, D., Rambal, S., Gaston, A. and Hiernaux, P.: 1995, A regional sahelian grassland model to be coupled with multispectral satellite data. I: Model description and validation, *Remote Sens. Environ.* **19**, 181–195.
10. Lo Seen D., Mougin, E., Rambal, S., Gaston, A. and Hiernaux, P.: 1995, A regional sahelian grassland model to be coupled with multispectral satellite data. II: Toward the control of its simulations by remotely sensed indices, *Remote Sens. Environ.* **52**, 194–206.
11. Iversen, J.D. and White, B.R.: 1982, Saltation threshold on Earth, Mars and Venus, *Sedimentology* **29**, 111–119.
12. Raupach, M.R.: 1991, Saltation layers, vegetation canopies and roughness lengths, *Acta Mech.* **1** (Suppl.), 83–96.
13. Raupach, M.R., Gillette, D.A. and Leys, J.F.: 1993, The effect of roughness elements on wind erosion threshold, *J. Geophys. Res.* **98**, 3023–3029.
14. Lettau, H.H.: 1969, Note on aerodynamic roughness-parameter estimation on the basis of roughness element description, *J. Appl. Meteorol.* **8**, 828–832.
15. Greeley, R. and Iversen, J.D.: 1985, *Wind as a Geological Process on Earth, Mars, Venus and Titan*, Cambridge University Press, New York, 333 pp.
16. Wooding, R.A., Bradley, E.F. and Marshall, J.K.: 1973, Drag due to regular arrays of roughness elements of varying geometry, *Boundary-Layer Meteorol.* **5**, 285–308.
17. Marshall, J.K.: 1971, Drag measurements in roughness arrays of varying density and distribution, *Agric. Meteorol.* **8**, 269–292.
18. Glendening, J.W.: 1977, *Aeolian Transport and Vegetative Capture of Particulates*, M.S. Thesis, Colorado State University, Fort Collins, CO.
19. Ash, J.E. and Wasson, R.J.: 1988, Vegetation and sand mobility in the Australian desert dunefield, *Zeitschrift für Geomorphologie Suppl. Bd.,* 45, 7–25, 1983. Eldridge, D.J., Soil-landform and vegetation relations in the chenopod shrublands of western New South Wales, *Earth Sci. Rev.* **25**, 493–499.

20. Musick, H.B and Gillette, D.A.: 1990, Field evaluation of relationships between a vegetation structural parameter and sheltering against wind erosion, *Land Degrad. Rehab.* **2**, 87–94.

21. Musick, H.B, Trujillo, S.M. and Truman, C.R.: 1996, Wind-tunnel modelling of the influence of vegetation structure on saltation threshold, *Earth Surf. Proc. Landforms* **21**, 589–605.

22. Marshall, J.K.: 1970, Assessing the protective role of shrub-dominated rangeland vegetation against soil erosion by wind, *Intern. Grassland Congr., 11th, Surfers Paradise (Australia)* **11**, 19–23.

23. Hoerner, S.F.: 1965, *Fluid Dynamic Drag*, S.F. Hoerner, Midland Park, NJ, 452 pp.

24. Schlichting, H.: 1968, *Boundary Layer Theory*, 6th edn., McGraw Hill, London and New York, NY, 747 pp.

25. Braun, H.: 1975, On the temperature dependence of constant temperature hot-wire probes with small wire aspect ratio. *J. Phys. E: Sci. Instrum.* **8**, 942–951.

26. Garratt, J.R.: 1977, *Aerodynamic Roughness and Mean Monthly Surface Stress over Australia*, Div. Atmos. Phys. Tech., Pap 29, CSIRO, Australia.

27. Hagen, L.J. and Lyles, L.: 1988, Estimating small grain equivalents of shrub dominated rangeland for wind erosion control, *Transactions of the ASAE.*

28. Jarvis, P.G., James, G.B. and Landsberg, J.J.: 1976, Coniferous forest, In: J.L. Monteith (ed.), *Vegetation and the Atmosphere*, Vol. 2, Academic Press, London, pp. 171–240.

29. Raupach, M.R., Thom, A.S. and Edwards, I.: 1980, A wind-tunnel study of turbulent flow close to regularly arrayed rough surfaces, *Boundary-Layer Meteorol.* **18**, 373–397.

30. Snyder, W.H.: 1979, *The EPA Meteorological Wind Tunnel: Its Design, Construction, and Operating Characteristics*. EPA-600/4-79-051. U.S. Environmental Protection Agency, Research Triangle Park.

31. Wolfe, S.A. and Nickling, W.G.: 1996, Shear stress partitioning in sparsely vegetated desert canopies, *Earth Surf. Proc. Landforms*, **21**, 607–619.

32. Wyatt, V.E. and Nickling, W.G.: 1997, Drag and shear stress partitioning in sparse desert creosote communities, *Can. J. Earth Sci.* **34**, 1486–1498.